Supplement of Atmos. Chem. Phys., 21, 12965–12988, 2021
https://doi.org/10.5194/acp-21-12965-2021-supplement

Atmospheric Chemistry and Physics
Open Access

Supplement of

Measurement report: Source apportionment of volatile organic compounds at the remote high-altitude Maïdo observatory

Bert Verreyken et al.

Correspondence to: Bert Verreyken (bert.verreyken@aeronomie.be)

1 hs-PTR-MS

1.1 Calibration coefficients

The 2-year variation on calibration coefficients throughout the deployment of the high-sensitivity quadrupole-based proton-transfer-reaction mass-spectrometry instrument (hs-PTR-MS) is shown in Figure S1. The discrete increases on 13/03/2018, 12–14/09/2018, 05–06/03/2019 are related to ion source/detector replacement. Other discrete increases in the calibration coefficients are mainly related to increases in the detector high voltage. The larger short-term variability of the calibration coefficients for isoprene, methyl vinyl ketone and methacrolein (MVK + MACR), methyl ethyl ketone, formic acid, and acetic acid reflects their dependence on air humidity.

During the OCTAVE intensive field campaign period, (March-May 2018), a hs-PTR-MS instrument from the Laboratoire des Sciences du Climat et de l'Environnement (LSCE) was deployed at La Réunion. Both instruments have been calibrated with the calibration systems foreseen by each institute (BISA and LSCE) to assure correct calibration of each instrument. The calibration coefficients obtained with our hs-PTR-MS from both calibration systems were found to be in good agreement (Figure S2).

1.2 Error analysis

Mixing ratios of the measured VOCs were obtained by dividing the background-subtracted normalized VOC ion signals (I_{net}, in ncps) by the respective interpolated calibration coefficients (C_{interp}, in ncps/ppbv). Normalization refers to VOC ion count rates that would be obtained at a source ion count rate of 10^6 cps. Whereas the error on the net normalized ion signals can be inferred from counting statistics, the error on the calibration coefficients was determined as described below. Regular 1-point calibrations (every 3-4 days) were performed by dynamic dilution of the calibration gas in zero-VOC air. The relative precision of those calibration coefficients is determined by the error on the normalized net VOC ion signals in the presence of calibration gas and varies from 0.6 to 2.1% between VOCs. Relative systematic errors include the reported uncertainty on the compound mixing ratios in the calibration bottle (5% at the 2σ level) and the error on the dilution factor (3.8% at the 2σ level). Every 2-3 months, calibrations were performed at different air humidities, controlled by a dew point generator (LI-610, LICOR). Of all compounds in the calibration mixture, only the calibration factors of isoprene (m/z 69), MVK+MACR (m/z 71), and methyl ethyl ketone (m/z 73) showed a non-negligible, albeit small dependence on air humidity. They varied linearly with the normalized $H_3O^+.H_2O$ ion signal (m/z 37), which was considered as a proxy of air humidity:

$$C = aI_{37} + b. \tag{1}$$

The slope a and corresponding standard error $\sigma(a)$ were obtained by linear regression, taking into account errors on I_{37} and C, and was assumed to remain constant in between calibrations versus relative humidity (roughly every 2 months). The b coefficients were then inferred for every regular calibration (every 3-4 days) from the measured calibration coefficient C and the average I_{37} signal during that calibration and the corresponding standard error $\sigma(b)$ was determined by standard error propagation.

Instantaneous calibration coefficients C_{interp} at time t were then obtained from Eq. 1, taking into account linearly interpolated b parameter values between the nearest regular calibrations and instantaneous I_{37} count rates.

The relative precision (RP) of the interpolated calibration coefficients is then given by Eq. 2, in which $x = \frac{t-t_l}{t_r-t_l}$, and $t_l(b_l)$ and $t_r(b_r)$ are the timestamps (b parameters) of the nearest calibrations before (suffix l) and after (suffix r) the ambient air measurement.

$$RP(C_{interp}) = \frac{\sigma(C_{interp})}{C_{interp}} = \frac{\sqrt{x^2\sigma^2(b_r) + (1-x)^2\sigma^2(b_l) + \sigma^2(a){I_{37}}^2}}{xb_r + (1-x)b_l + aI_{37}} \tag{2}$$

The relative expanded uncertainty on the calibration coefficients is obtained by combining the relative precision of the interpolated calibration coefficients and the relative systematic errors on the dynamic calibration gas dilution factor in the calibration set-up and on the mixing ratio of the compounds in the calibration gas bottle.

Median values for the instantaneous calibration factors, their relative precision and relative total expanded uncertainty for the compounds that are present in the calibration bottle are shown in Table S1.

compound	m/z	C_{interp} (ncps/ppbv)	$RP(C_{interp})$ (%) (1σ)	Relative expanded uncertainty of C_{interp} (%) (k=2)
methanol	33	10.20	0.73	6.45
acetaldehyde	45	12.72	0.61	6.40
acetonitrile	42	15.04	0.77	6.46
acetone	59	15.05	0.51	6.36
DMS	63	8.10	0.73	6.45
isoprene	69	3.42	3.13	8.87
MVK+MACR	71	9.09	0.99	6.58
MEK	73	12.10	1.23	6.74
benzene	79	7.07	0.92	6.54
m-xylene	107	6.08	1.27	6.78
limonene	137	1.39	1.48	6.95

Table S1: Median values for the instantaneous calibration factors, their relative precision and relative expanded uncertainty for the compounds that are present in the calibration bottle.

1.2.1 Formic and acetic acid

Calibration coefficients of acetic acid, C_{AA}, based on the hs-PTR-MS ion signal at m/z 61 have been inferred from those of acetone, $C_{acetone}$ (which were measured regularly), by taking into account the calculated collision rate constants (k) of H_3O^+ ions with acetic acid and acetone (Su, 1994; Zhao and Zhang, 2004), the instrument transmission at m/z 59 (protonated acetone, T_{59}) and at m/z 61 (protonated acetic acid, T_{61}), and the transmission-corrected fractional contribution of m/z 61 ions (F_{61}) to the H_3O^+/acetic acid product ion distribution (Eq. 3). The H_3O^+/acetone reaction was assumed to proceed solely by non-dissociative proton transfer and the transmission factors at m/z 59 and m/z 61 were assumed to be equal, as the mass to charge ratios are very close to each other. F_{61} was obtained by sampling a dynamically diluted mixture of acetic acid (starting from the headspace of the pure compound) in zero-VOC air at different air humidities, (controlled by the dew point generator) and was found to be strongly humidity-dependent and in good agreement with the literature (Baasandorj et al., 2015).

$$C_{AA} = \frac{k_{AA}}{k_{acetone}} \times \frac{T_{61}}{T_{59}} \times F_{61} \times C_{acetone} \quad (3)$$

Whereas the relative precision of $C_{AA,interp}$ is mainly determined by the relative precision of $C_{acetone,interp}$ (0.5 %, 1σ), the relative expanded uncertainty of C_{interp} (k=2) is largely determined by the systematic errors on the rate constants (15%, 1σ) and on F_{61} (5%, 1σ) and is estimated to be as large as 43%. Formic acid calibration factors C_{FA} at m/z 47 were calculated in a similar way, but using acetaldehyde (m/z 45) as a reference compound, which also reacts with H_3O^+ by non-dissociative proton transfer. In contrast to acetic acid, proton transfer to formic acid only results in the protonated molecule (F_{47}=1). Nevertheless, Baasandorj et al. (2015) have shown that the calibration coefficient for formic acid still shows a large humidity dependence. This was taken into account by multiplying the C_{FA} values by the function expressing the variation of the Baasandorj et al. (2015) calibration factors versus $I_{m/z37}/I_{m/z19}$, normalized with respect to zero humidity. This function was obtained with a similar hs-PTR-MS instrument and at similar operating conditions. Similar as for acetic acid, the relative precision and relative expanded uncertainty (k=2) of $C_{FA,interp}$ were estimated to be 0.6 (1σ) and 43%, respectively.

1.3 Data quality

The data quality is represented in plots shown in Figure S3. The average signal-to-noise ratio (S/N) or a sample is computed putting a maximum of 10 for each data entry in the sample set in order to avoid excessive influence from strong pollution plumes related to e.g. biomass burning. When looking at the quality of data at the location of Maïdo, it is important to take the effects of mesoscale transport into account. Thermally driven mesoscale transport features result in the observatory being located in the planetary boundary layer (PBL) during daytime. During nighttime however, the observatory is predominantly located in air masses originating at higher altitudes in the free troposphere (FT). As a result, nighttime air-masses are much less affected by local sources located on the island and the expected mixing ratios in the FT are much lower than

during the daytime. This is reflected in the difference in the quality of data between nighttime and daytime measurements (Figure S3).

2 Measurements

2.1 PTR-MS

As the seasonal differences in the paper are discussed often using monthly variation, we show the monthly averages in figure S4.

2.2 PMF

In order to use the PMF algorithm, the hs-PTR-MS dataset was split into three random subsets to be analysed separately. For this, each data point was assigned a label assigning it to a particular subset. This assigning was done randomly and it is important to note that the different sources contribute equally to each subset of data. This was most critical for biomass burning as this depends largely on spurious increases of VOC mixing ratios recorded with the hs-PTR-MS instrument when a biomass burning plume was advected directly from a source in southern Africa or Madagascar towards the location of Maïdo. As an illustration, a subset of acetonitrile data during August 2018 is shown in Figure S5. It is important here to note that every datapoint can only be attributed to 1 subset and that all three subsets are sampling increases of acetonitrile related to biomass burning plumes reaching the observatory.

An additional plot showing pollution roses for all four of the identified source factors is shown in Figure S6. We see that the behaviour described in the manuscript is confirmed with a relatively homogeneous distribution for both the primary biogenic and background source factors but with a clear source located East/West of the observatory for the secondary biogenic/anthropogenic source factors respectively.

References

Baasandorj, M., Millet, D. B., Hu, L., Mitroo, D., and Williams, B. J.: Measuring Acetic and Formic Acid by Proton-Transfer-Reaction Mass Spectrometry: Sensitivity, Humidity Dependence, and Quantifying Interferences, Atmospheric Measurement Techniques, 8, 1303–1321, https://doi.org/10.5194/amt-8-1303-2015, 2015.

Su, T.: Parametrization of Kinetic Energy Dependences of Ion–Polar Molecule Collision Rate Constants by Trajectory Calculations, J. Chem. Phys., 100, 4703–4703, https://doi.org/10.1063/1.466255, 1994.

Zhao, J. and Zhang, R.: Proton transfer reaction rate constants between hydronium ion (H3O+) and volatile organic compounds, Atmospheric Environment, 38, 2177–2185, https://doi.org/https://doi.org/10.1016/j.atmosenv.2004.01.019, 2004.

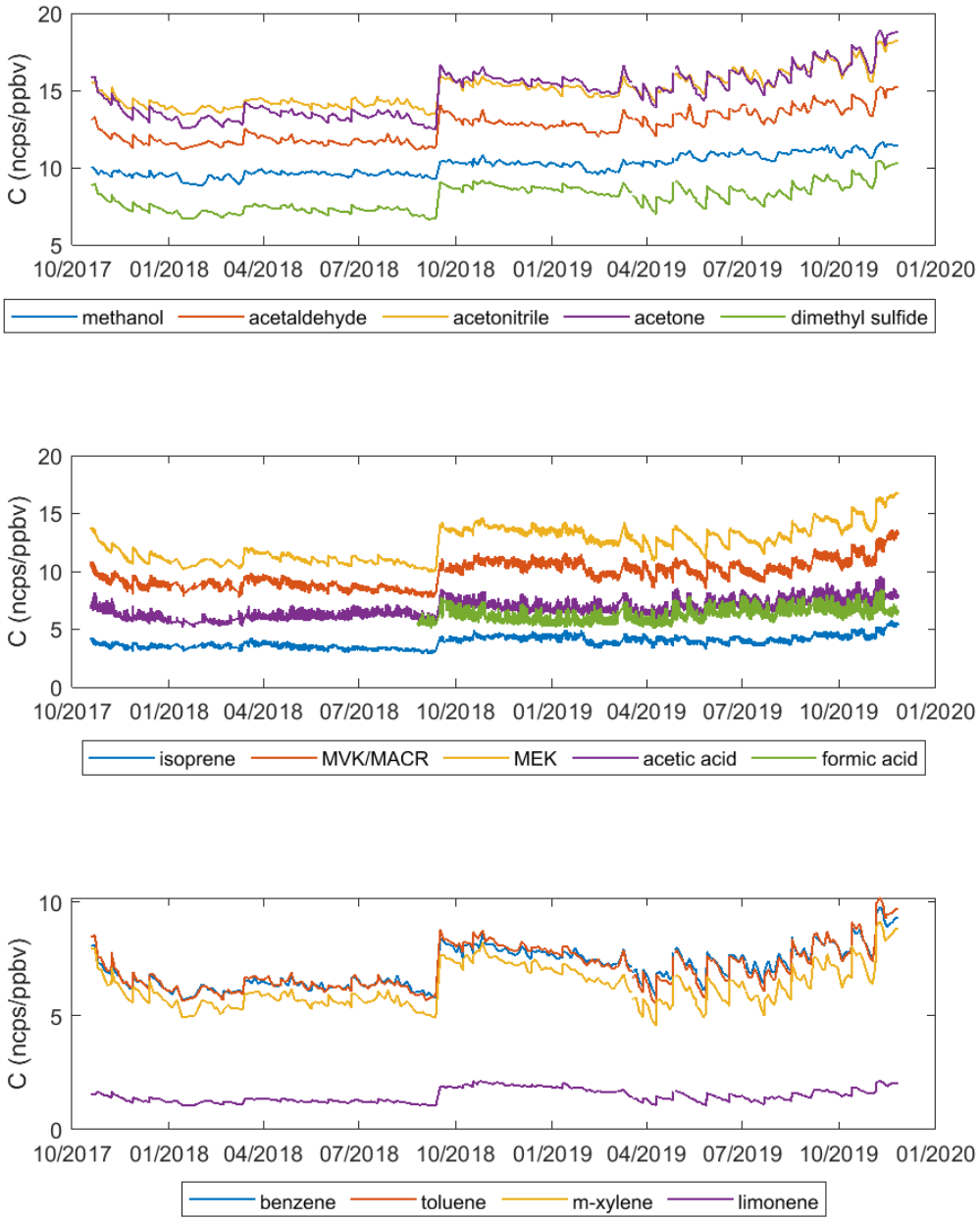

Figure S1: Instantaneous calibration coefficients (ncps/ppbv) for the measured compounds.

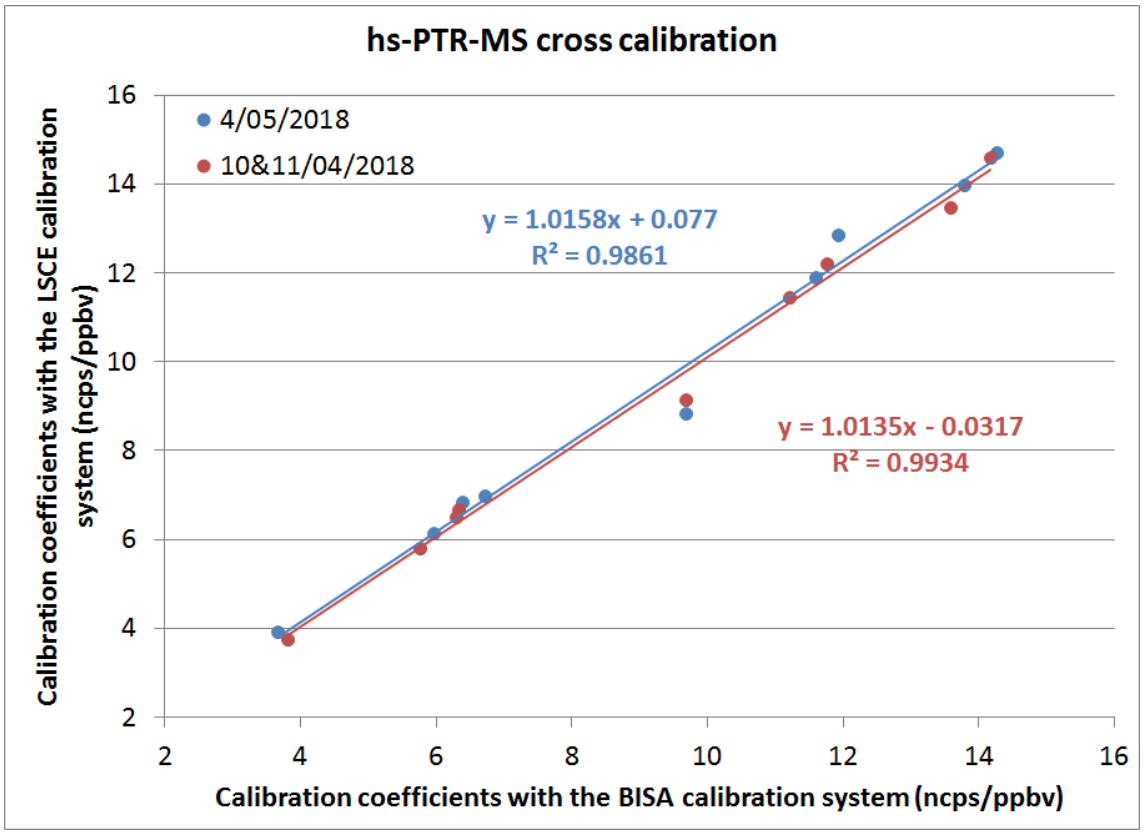

Figure S2: Correspondence between calibration factors obtained with the custom-built BISA hs-PTR-MS calibration system and the commercial Ionicon gas calibration unit from LSCE for the BISA hs-PTR-MS instrumen (05/04, 10 and 11/04). Species that were present in both calibration systems and thus suitable for the cross calibration purposes here were methanol, acetonitrile, acetaldehyde, acetone, isoprene, 2-butanone, benzene, toluene, and xylene.

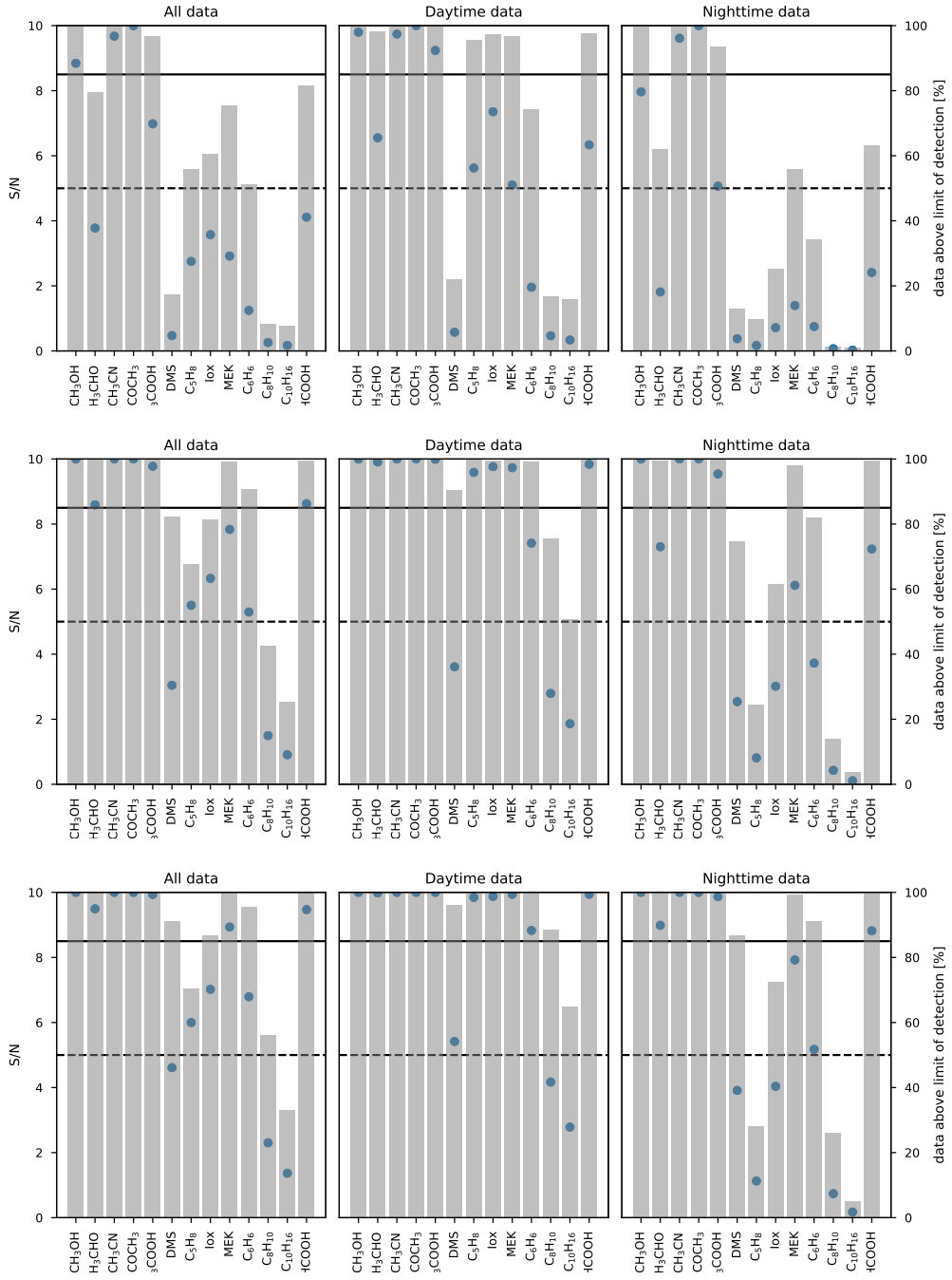

Figure S3: Signal-to-noise ratio (S/N, blue markers) and the fraction of data above limit of detection (LoD, gray bars) for hs-PTR-MS data throughout the entire 2-year OCTAVE campaign. Top row shows the data quality for individual measurements, the middle and bottom rows show the data quality for aggregated data over 30 and 60 minute intervals respectively. The effective dwell times for the aggregated data is equivalent to about 110 and 220 s for the 30 minute and 60 minute intervals respectively. The leftmost column shows data quality taking into account all data, the middle column shows the data quality during the daytime interval (10:00 – 17:00 LT) while the rightmost column illustrates quality during the nighttime (22:00 – 05:00 LT).

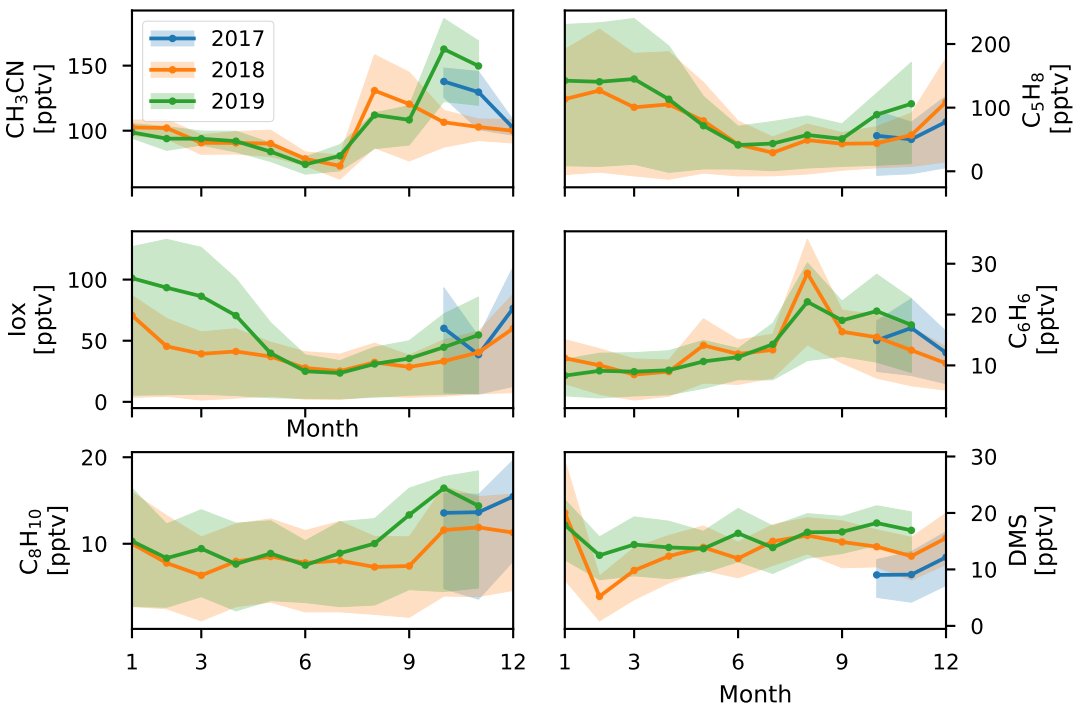

Figure S4: Monthly average values of CH_3CN, C_5H_8, Iox, C_6H_6, C_8H_{10}, and DMS (top to bottom) for 2017, 2018, and 2019 (blue, orange and green respectively) during the deployment of the hs-PTR-MS instrument for the OCTAVE project. Shaded areas behind the curve show the monthly interquartile range. Plot constructed using halfhourly averages.

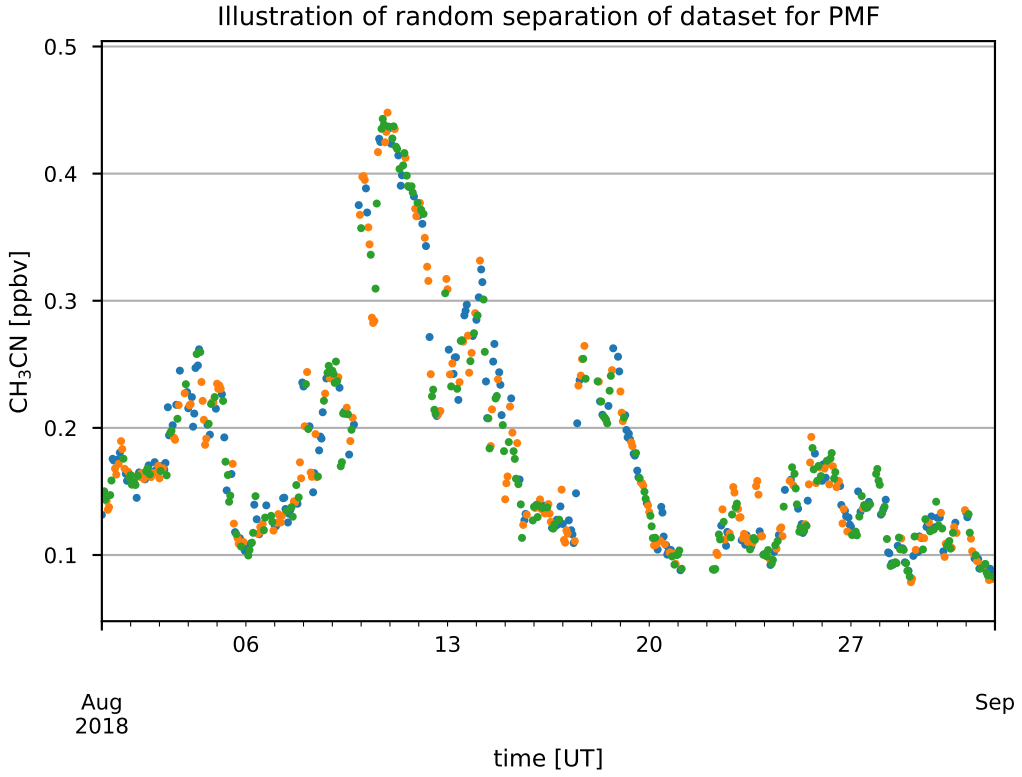

Figure S5: Acetonitrile concentrations and how the datapoints are distributed over the 3 random subsets of data that were analysed using PMF.

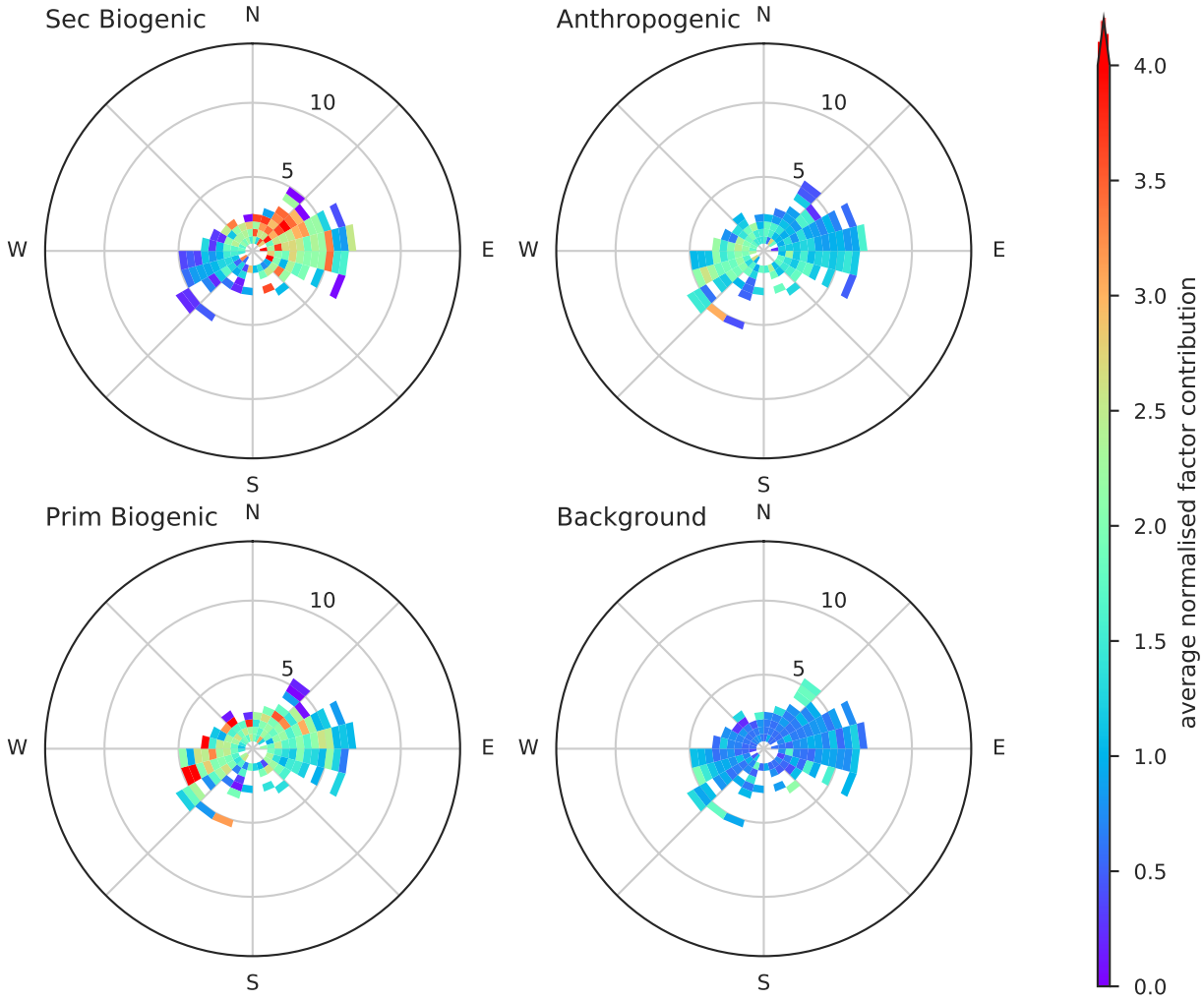

Figure S6: Daytime (10:00 – 17:00 LT) pollution roses for each of the four factors identified using the PMF algorithm. The average normalised contribution on a grid using 15° resolution in direction (polar axis) and 0.5 m/s resolution in wind speed (radial axis) is shown for the secondary biogenic (top left), primary biogenic (bottom left), anthropogenic (top right), and background (bottom right) source factors.